Growth mechanism and blue shift of Mn^{2+} luminescence for wurtzite $ZnS:Mn^{2+}$ nanowires

2010 J. Phys. D: Appl. Phys. 43 075403

(http://iopscience.iop.org/0022-3727/43/7/075403)

IOP PUBLISHING JOURNAL OF PHYSICS D: APPLIED PHYSICS

J. Phys. D: Appl. Phys. **43** (2010) 075403 (6pp) doi:10.1088/0022-3727/43/7/075403

Growth mechanism and blue shift of Mn^{2+} luminescence for wurtzite ZnS : Mn^{2+} nanowires

Jian Cao[1,2], Jinghai Yang[3], Yongjun Zhang[3], Lili Yang[3], Dandan Wang[1,2], Maobin Wei[3], Yaxin Wang[3], Yang Liu[3], Ming Gao[3] and Xiaoyan Liu[3]

[1] Key Laboratory of Excited State Physics, Changchun Institute of Optics, Fine Mechanics and Physics, Chinese Academy of Sciences, 3888 Eastern Nan-Hu Road, Changchun 130033, People's Republic of China

[2] Graduate School of the Chinese Academy of Sciences, Beijing, 100049, People's Republic of China

[3] Institute of Condensed State Physics, Jilin Normal University, Siping 136000, People's Republic of China

E-mail: jhyang1@jlnu.edu.cn

Received 31 October 2009, in final form 7 January 2010
Published 4 February 2010
Online at stacks.iop.org/JPhysD/43/075403

Abstract

Wurtzite-type ZnS : Mn^{2+} nanowires were prepared by a hydrothermal method at 180 °C without any surface-active agent. The structure and morphology of the samples were characterized by x-ray diffraction, transmission electron microscopy, high-resolution transmission electron microscopy, Fourier transform infrared spectroscopy and energy dispersive spectroscopy. The average diameter of the nanowires was about 10 nm. An ethylenediamine-mediated template was observed and employed to explain the growth mechanism in detail. A strong yellow–orange emission from the Mn^{2+} $^4T_1$–$^6A_1$ transition was observed in the photoluminescence spectra, which exhibited blue shift as the Mn^{2+} doped ratio increased.

(Some figures in this article are in colour only in the electronic version)

1. Introduction

One-dimensional (1D) nanostructures (nanorods, nanowires, nanobelts) have attracted tremendous attention because of their proven potential use as both interconnects and functional units in electronic, optoelectronic, electrochemical and electromechanical devices [1, 2]. Zinc sulfide (ZnS) is an important wide band gap (E_g = 3.6 eV at 300 K) semiconductor, which is considered important for applications such as ultraviolet-light-emitting diodes, electroluminescent devices, flat-panel displays, sensors and injection lasers [3–7]. Under ambient conditions, ZnS has two types of polymorphs: zinc blende (cubic) and wurtzite (hexagonal). The cubic ZnS is stable at room temperature, whereas the hexagonal ZnS is stable at temperatures higher than 1020 °C. When doped with some metal cations (including transition metal ions and rare-earth elements), ZnS usually exhibits a variety of luminescent properties, such as photoluminescence (PL), electroluminescence, thermoluminescence and triboluminescence [8–11]. Among these elements, Mn doping in ZnS attracts a great deal of interest since Mn doping can not only enhance its optical transition efficiency and increase the number of luminescent centres, but can also inspire the material to exhibit interesting magneto-optical properties [12–15], which is obviously an effective way to enhance the properties for ZnS practical application. As for the 1D cubic ZnS : Mn^{2+} nanomaterials, Chaudhuri and co-workers [16] have synthesized ZnS : Mn^{2+} nanorods at 200 °C with a solvothermal method, and Mandal *et al* [17] have obtained ZnS : Mn^{2+} nanorods within the pores of a polycarbonate membrane. As for the 1D wurtzite ZnS : Mn^{2+} nanomaterials, Li and co-workers [18] have reported a halide-transport chemical vapour deposition (HTCVD) method to fabricate ZnS : Mn^{2+} nanobelts and nanowires at 750 °C, and Yan and co-workers [19] have reported the synthesis of ZnS : Mn^{2+}

nanowires by a chemical vapour deposition technique at 700 °C using Zn and S powders as precursors. Although the synthesis of 1D wurtzite $ZnS:Mn^{2+}$ nanomaterials always required rigid experimental conditions, owing to its excellent optical properties, it is still much more desirable than the 1D cubic $ZnS:Mn^{2+}$ nanomaterials. So, exploring the low-temperature (below 200 °C) synthesis technique for highly crystalline 1D wurtzite $ZnS:Mn^{2+}$ nanomaterials has always been a hot and challenging topic.

In this paper, we present a simple hydrothermal method to synthesize wurtzite $ZnS:Mn^{2+}$ nanowires. This method can be carried out at a relatively low temperature with quite cheap precursors of low toxicity, and the most important thing is that it is easier to incorporate the transition metal ions such as Mn^{2+} and Cu^{2+} into the ZnS lattice. Ethylenediamine (EN) and water were used as the solvents in our experiments. Since EN can easily react with Zn and S to form the intercalated lamellar compound $ZnS{\cdot}EN_{0.5}$ [20], which can be decomposed into different morphologies under different conditions [21–25]. To the best of our knowledge, few detailed investigations were reported on the structural evolvement process from the $ZnMnS{\cdot}EN_{0.5}$ precursor to the wurtzite $ZnS:Mn^{2+}$ nanowires. Therefore, it is meaningful to investigate the formation mechanism of wurtzite $ZnS:Mn^{2+}$ nanowires, which can provide useful information on the morphology-controlled synthesis of wurtzite $ZnS:Mn^{2+}$ nanostructures and other inorganic nanostructures. In addition, the results from PL measurement indicated that the PL intensity was enhanced and a blue shift was exhibited as the Mn^{2+} doping concentration increased in the wurtzite $ZnS:Mn^{2+}$ nanowires.

2. Experimental

$Zn_{1-x}Mn_xS$ ($x = 0$, 0.01, 0.05) nanowires were prepared by the hydrothermal technique. In our experiments, all chemicals were of analytical grade and were used as received without further purification. The total amount of $Zn(NO_3)_2{\cdot}6H_2O$ and $Mn(NO_3)_2$ was 0.5 mmol. First, $Zn(NO_3)_2{\cdot}6H_2O$ and $Mn(NO_3)_2$ in appropriate proportions were dissolved in 16 ml EN and water (1 : 1 in volume ratio). After stirring for 1 h, NH_2CSNH_2 (1.5 mmol) was added into the resulting complex. After stirring for 2 h, the colloid solution was transferred into a 20 ml Teflon-lined autoclave and kept at 180 °C for 12 h. After the reaction, the autoclave was taken out and cooled down to room temperature. The product was washed with ethanol and deionized water for several times and separated by centrifugation, and then dried at 80 °C for 1 h to get a white powder. To investigate the growth mechanism of the nanowires, we also prepared the sample ($x = 0.01$) at 180 °C for 4 h and 8 h, respectively.

The x-ray diffraction (XRD) pattern was collected on a MAC Science MXP-18 x-ray diffractometer using a Cu target radiation source. A transmission electron micrograph (TEM) was taken with a JEM-2100 electron microscope. The specimen was prepared by depositing a drop of the dilute solution of the sample in 2-propanol on a carbon-coated copper grid and drying at room temperature. The Fourier transform infrared (FT-IR) spectrum was recorded on a Bruker Vertex 70 spectrophotometer using KBr pellets. The UV–Vis absorption spectrum was measured on a UV-3101PC UV spectrometer. The specimen for the measurement was dispersed in ethanol and placed in a 1 cm quartz cell, and ethanol served as the reference. PL measurement was carried out at room temperature, using 325 nm as the excitation wavelength, and He–Cd laser as the source of excitation. The PL excitation spectrum was recorded at room temperature using a Hitachi F-4500 spectrophotometer equipped with a continuous 150 W Xe-arc lamp.

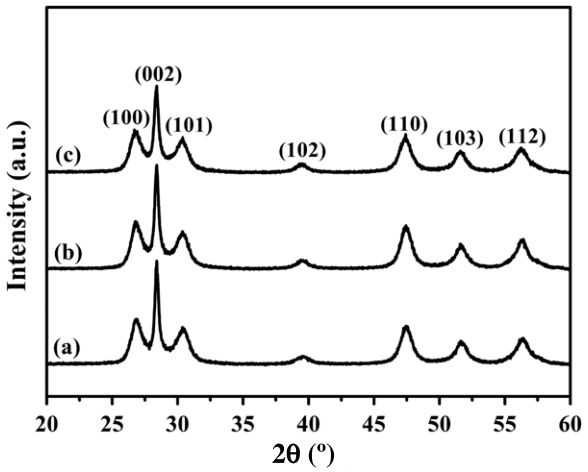

Figure 1. XRD patterns of (a) ZnS, (b) $Zn_{0.99}Mn_{0.01}S$ and (c) $Zn_{0.95}Mn_{0.05}S$ nanowires.

3. Results and discussion

The XRD patterns of $Zn_{1-x}Mn_xS$ ($x = 0$, 0.01, 0.05) nanowires are shown in figure 1. All the diffraction peaks can be well indexed as hexagonal wurtzite phase structure, which are consistent with the standard card (JCPDS No 36-1450). The growth direction could be predicted by comparing the full-width at half-maxima (FWHM) of the different diffraction peaks [26]. Note that the (0 0 2) diffraction peak is stronger and narrower than the other peaks, suggesting a preferential growth direction along the *c*-axis, which is further demonstrated below by TEM and HRTEM studies. Moreover, the doping of Mn^{2+} ions has no significant effect on the structure of ZnS nanowires, which indicates that Mn^{2+} ions may be incorporated into the ZnS lattice.

To investigate the growth mechanism of $ZnS:Mn^{2+}$ nanowires, we display TEM and HRTEM images of the $Zn_{0.99}Mn_{0.01}S$ nanowires grown for 4 h in figures 2(*a*) and (*b*). We can observe that the nanowires exist in the form of a $ZnMnS{\cdot}EN_{0.5}$ template (figure 2(*a*)), and its growth direction is close to the *c*-axis but not along the *c*-axis (figure 2(*b*)), which can be further verified by XRD results later. Figures 2(*c*) and (*d*) show the enlarged image of the clear boundaries 1 and 2 in figure 2(*b*), respectively. With growth time increasing, these boundary regions would detach from each other and serve as the seed for the growth of the uniform nanowires. As seen from the XRD patterns of the $Zn_{0.99}Mn_{0.01}S$ nanowires grown for 4 and 8 h (figure 2(*h*)), the positions of all the

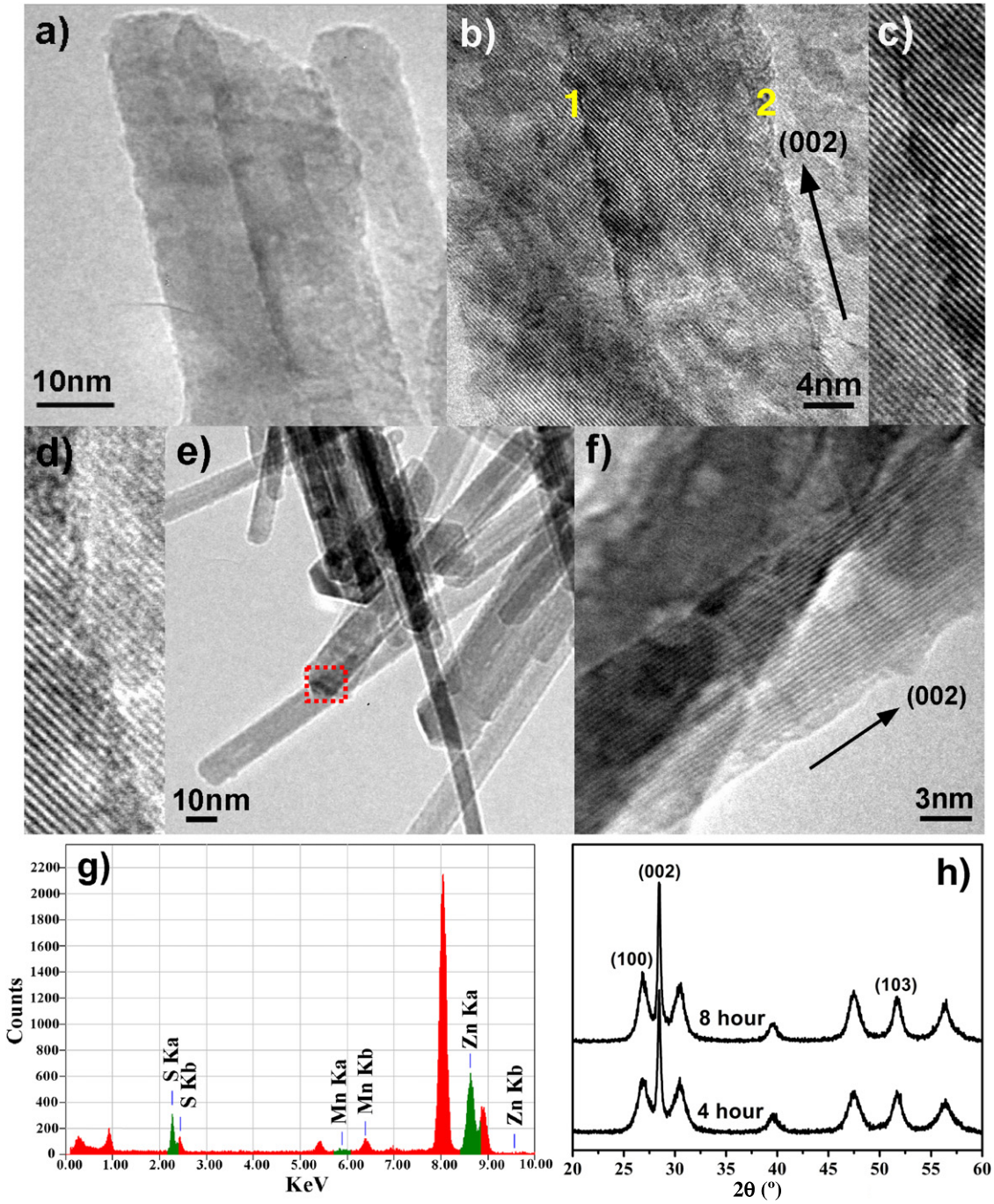

Figure 2. (*a*), (*b*) TEM and HRTEM images of the $Zn_{0.99}Mn_{0.01}S$ nanowires grown for 4 h; (*c*), (*d*) the enlarged images of boundaries 1 and 2 in (*b*); (*e*), (*f*) TEM and HRTEM images of the $Zn_{0.99}Mn_{0.01}S$ nanowires grown for 12 h; (*g*) EDS spectrum of the $Zn_{0.99}Mn_{0.01}S$ nanowires grown for 12 h; (*h*) XRD patterns of the $Zn_{0.99}Mn_{0.01}S$ nanowires grown for 4 and 8 h.

diffraction peaks for the two samples are consistent with that for the sample grown for 12 h (figure 1(b)). Consequently, we can deduce that, after reacting up to 4 h, the wurtzite $Zn_{0.99}Mn_{0.01}S$ nanomaterials have already formed. But it is worth noting that the change in intensity of each diffraction peak is different. The (0 0 2) diffraction peak is stronger and narrower than the other peaks, which does not show a clear change with the extension of the reaction time. Whereas the intensity of the (1 0 0) and (1 0 3) diffraction peak is increased and decreased, respectively, which further demonstrates that the growth direction of the nanowires is not along the (0 0 2) direction at the initial stage of the reaction. This can be attributed to the different growth trends of the individual lattice planes, here, referring to the (0 0 2), (1 0 0) and (1 0 3) lattice planes.

Figures 2(*e*) and (*f*) show the TEM and HRTEM images of the $Zn_{0.99}Mn_{0.01}S$ nanowires grown for 12 h. The TEM image (figure 2(*e*)) shows that these wires are smooth and uniform over their entire length and the average diameter is about 10 nm. Compared with the sample grown for 4 h, the diameter of the nanowires does not change much, revealing that the size of the nanowires can be determined by the

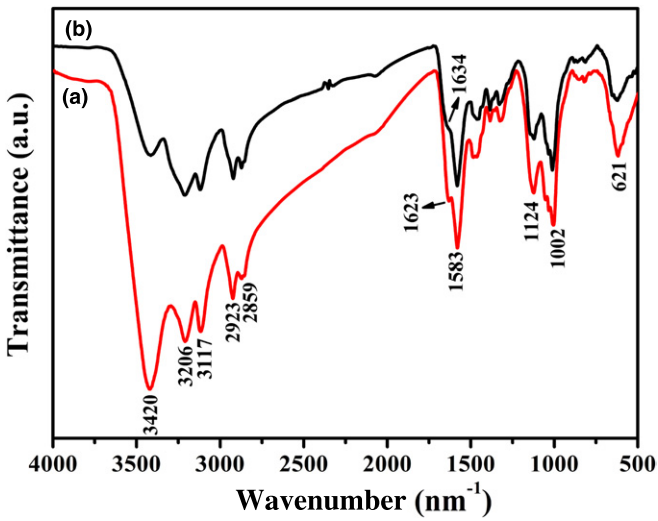

Figure 3. FT-IR spectra of (a) ZnS and (b) $Zn_{0.99}Mn_{0.01}S$ nanowires.

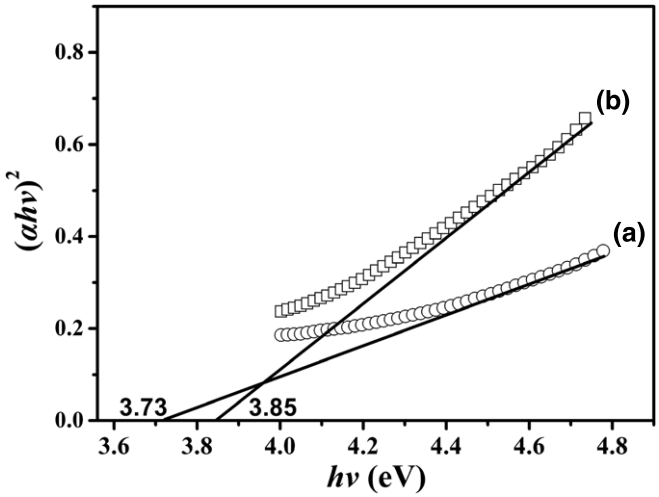

Figure 4. Plots of $(\alpha h\nu)^2$ versus $h\nu$ for (a) ZnS and (b) $Zn_{0.99}Mn_{0.01}S$ nanowires.

$ZnMnS{\cdot}EN_{0.5}$ template formed in the reaction. The HRTEM image (figure 2(f)) of the single wire marked in figure 2(e) shows that the sample grows along the (0 0 2) direction, which is well oriented with good crystallization.

On the basis of the above structure analysis of the samples grown for different times, the possible growth mechanism can be described as follows: first, thiourea released S^{2-} ions slowly with the aid of EN when the solution was sealed in Teflon at the reaction temperature (180 °C) (equation (1)) [27–29], and then EN connected with Zn^{2+}, Mn^{2+} and S^{2-} ions to form the $ZnMnS{\cdot}EN_{0.5}$ template (equation (2)).

$$(NH_2)_2CS + 2OH^- \rightarrow S^{2-} + 2NH_3 + CO_2, \quad (1)$$

$$ZnMnS \cdot EN_{0.5} \rightarrow ZnMnS \downarrow +0.5EN. \quad (2)$$

Under the hydrothermal condition, the templates dissociated from each other at the boundary regions, eliminating the EN molecules from the $ZnMnS{\cdot}EN_{0.5}$ template. These detached wires would grow along the (0 0 2) direction, which are consistent with the anisotropic wurtzite structure, i.e. the unique structural feature of the (0 0 1 h) facet and the existence of a 63-screw axis along the c-direction (Donnay–Harker law) [21, 30, 31]. The energy dispersive spectroscopy (EDS) spectrum (figure 2(g)) shows that the $Zn_{0.99}Mn_{0.01}S$ nanowires contain Zn, S and Mn elements, and 0.7 at% Mn is detected in the sample.

FT-IR spectra of ZnS and $Zn_{0.99}Mn_{0.01}S$ nanowires are shown in figure 3 to further ascertain the presence of the $ZnMnS{\cdot}EN_{0.5}$ template. The presence of the bands around 2900–3420 and 1623 cm^{-1} can be assigned to the N–H deformation vibration, demonstrating the existence of EN molecules on the surface of the nanowires [32–34]. Note that the peak at 1623 cm^{-1} for the ZnS nanowires is at a lower wavenumber than that for the $Zn_{0.99}Mn_{0.01}S$ nanowires (at 1634 cm^{-1}), indicating that there is a relatively strong interaction between the EN molecules and the surface of the $Zn_{0.99}Mn_{0.01}S$ nanowires [35]. Consequently, during the reaction, the proposed EN-mediated template is formed by immobilizing the NH_2 bimolecule through covalent bonding. In addition, the bands at 2850–2923 and 1300–1400 cm^{-1} can be assigned to the stretching vibrations and bending vibrations of C–H [33, 36]. The bands at 1127 cm^{-1} and 621 cm^{-1} can be assigned to the C–O symmetric vibration [36] and the C–S symmetric vibration [34], respectively.

The optical band gap E_g can be calculated using the following relation:

$$\alpha = A(h\nu - E_g)^n / h\nu,$$

where A is a constant and n is a constant, equal to 1/2 for the direct band gap semiconductor. The plots of $(\alpha h\nu)^2$ versus $h\nu$ for ZnS and $Zn_{0.99}Mn_{0.01}S$ nanowires are shown in figure 4. The linear nature of the plot indicates the existence of the direct transition. The band gap E_g is determined by extrapolating the straight portion to the energy axis at $\alpha = 0$. It is found to be 3.73 eV for ZnS and 3.85 eV for $Zn_{0.99}Mn_{0.01}S$ nanowires, which are blue-shifted compared with the bulk ZnS (3.65 eV), indicating that the diameter of the nanowires is near the quantum-confined regime [25, 37]. Moreover, after doping Mn^{2+} ions into the ZnS lattice, the peak position has a 0.12 eV blue shift. A possible explanation is based on the modified effect of the Mn^{2+} ions on the electronic structure of ZnS nanowires. According to Albe *et al* [38], within the tight-binding framework, the doping effect can modify the highest valence state (weak) and the lowest conduction state (strong) and thereby widen the band gap.

The PL spectrum of the ZnS nanowires (figure 5(a)) shows a broad emission band between 2 and 3.5 eV that can be decomposed into six Gaussian peaks centred at 2.18 eV, 2.31 eV, 2.55 eV, 2.76 eV, 2.91 eV and 3.08 eV, respectively. According to the energy diagram of the defects distributed in the ZnS [16], the emission peaks can be attributed to the following origins: 3.08 eV to interstitial S [39], 2.91 and 2.76 eV to S vacancy and surface states [25, 40], 2.55 eV to Zn vacancy [25] and 2.31 eV to sulfur species on the surface of the ZnS nanowires [41]. We would like to point out that the emission peak at 2.18 eV is rarely observed by others. Only Li *et al* [41] and Yao *et al* [42] have observed this

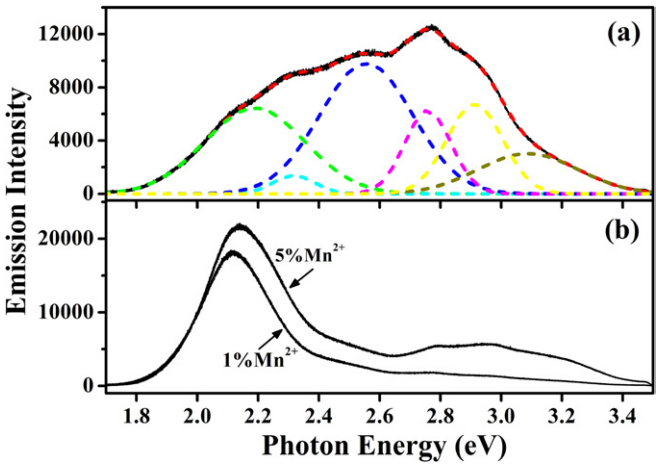

Figure 5. PL spectra of (*a*) ZnS and (*b*) $Zn_{0.99}Mn_{0.01}S$ and $Zn_{0.95}Mn_{0.05}S$ nanowires.

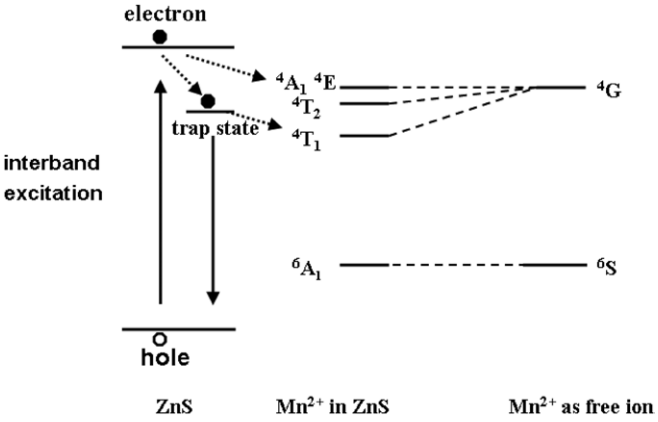

Figure 6. Energy level diagram of ZnS : Mn^{2+} and free Mn^{2+} ions.

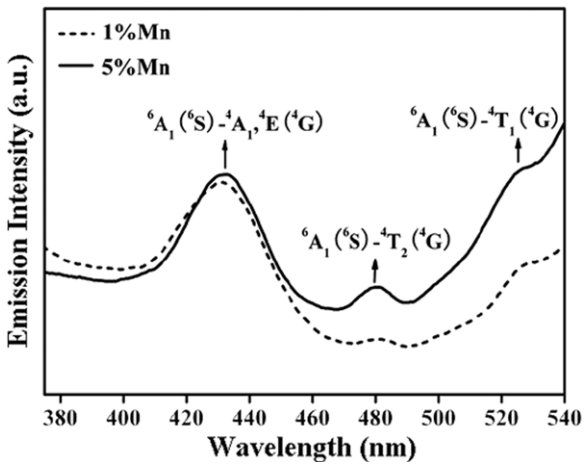

Figure 7. PL excitation spectra of the Mn^{2+} ions in $Zn_{0.99}Mn_{0.01}S$ (dashed curve) and $Zn_{0.95}Mn_{0.05}S$ (solid curve) nanowires.

peak in wurtzite ZnS nanosheets and special flower spheres. So its origin is still not clear and needs further study. In the PL spectra of $Zn_{1-x}Mn_xS$ ($x = 0.01$, 0.05) nanowires (figure 5(*b*)), both blue (weak) and yellow–orange (strong) emissions can be observed and the dominant yellow–orange emission is from the Mn^{2+} $^4T_1$–$^6A_1$ transition. Sooklal *et al* [43] have studied the effect of the location of the Mn^{2+} ions on the photophysics of ZnS nanomaterials. They found that the Mn^{2+} ions incorporated into the ZnS lattice would lead to the yellow–orange emission, while the Mn^{2+} ions distributed on the surface of ZnS would yield the ultraviolet emission. As a comparison with our results, we can suggest that the Mn^{2+} ions are incorporated into the ZnS lattice occupying the tetrahedral cationic site in Td symmetry. Under this symmetry, the first excited state ^4G of the free Mn^{2+} ions splits into $^4T_1$, $^4T_2$, $^4A_1$ and ^4E multiplet states ($^4A_1$ and ^4E states are degenerate), as seen in figure 6. According to Bhargava *et al* [44], when Mn^{2+} ions are incorporated into the ZnS lattice substituting the Zn sites, mixing between the sp electrons of the ZnS host and the d electrons of the Mn^{2+} ions occurs, which makes the forbidden transition of $^4T_1$–$^6A_1$ partially allowed, resulting in the characteristic emission of Mn^{2+} ions. As the Mn^{2+} doped ratio increased, the intensities of the yellow–orange and the blue emissions are increased. Because the Mn^{2+} ions would capture more electron–hole pairs and emit more photons [18, 45], leading to the enhancement of the yellow–orange emission, meanwhile more Mn^{2+} ions would stay at the surface or interstitial positions of the crystal with an octahedral symmetry, which is favourable for the blue emission. It is noticeable that the yellow–orange emission shifts towards the higher energy region as the Mn^{2+} doped ratio increased, i.e. blue shift occurs. This can be explained by the energy transfer process in $Zn_{1-x}Mn_xS$ nanowires. According to Sarma and co-workers [46], the excitation pathway for the dopant site has two ways (figure 6), namely the energy transfers directly from the host to the Mn^{2+} d states and another from the defect sites to the Mn^{2+} d states. Figure 7 shows the PL excitation spectra of the Mn^{2+} ions in $Zn_{0.99}Mn_{0.01}S$ and $Zn_{0.95}Mn_{0.05}S$ nanowires, which were obtained by monitoring the emission peaks at 2.11 eV and 2.14 eV, respectively. The sharp lines in figure 7 are associated with the d–d transitions of the Mn^{2+} ions. Their detailed origins have been labelled. It is apparent that the intensity of the excitation peak ($^4T_1$–$^6A_1$) for the $Zn_{0.95}Mn_{0.05}S$ nanowires is stronger than that for the $Zn_{0.99}Mn_{0.01}S$ nanowires. This could be attributed to the variation of coordination environments around the Mn^{2+} ions in the two samples, which would affect the energy transfer process. Therefore, our results support the idea that there is an energy transfer from the defect states to the Mn^{2+} states in terms of the blue shift, as has been discussed by Vijay and co-workers [47]. However, to the best of our knowledge, very few reports have been published on the blue shift of Mn^{2+} luminescence for wurtzite ZnS : Mn^{2+} nanowires. Hence, the exact mechanism needs to be further studied.

4. Conclusion

In summary, wurtzite-type ZnS : Mn^{2+} nanowires have been synthesized by the simple hydrothermal method at a low temperature of 180 °C. The wires grew along the (0 0 2) direction. An EN-mediated template was formed in the reaction, which would determine the size of the nanowires. The yellow–orange emission from the Mn^{2+} $^4T_1$–$^6A_1$ transition was observed and the peak position of the Mn^{2+} emission

exhibited blue shift as the Mn^{2+} doped ratio increased, which apparently prompted their applications in nanoscale optoelectronic devices.

Acknowledgments

This work was financially supported by the National Natural Science Foundation of China (Grant No 60778040, 60878039, 10904050), National Programmes for High Technology Research and Development of China (863) (Item No 2009AA03Z303), Programme for the Development of Science and Technology of the Jilin province (Item No 20082112).

References

[1] Yin L and Bando Y 2005 *Nature Mater.* **4** 883
[2] Xing G Z *et al* 2008 *Adv. Mater.* **20** 3521
[3] Zhu Y F, Fan D H and Shen W Z 2008 *J. Phys. Chem.* C **112** 10402
[4] Quan Z, Yang D, Li C, Kong D, Yang P, Cheng Z and Lin J 2009 *Langmuir* **25** 10259
[5] Sun Q, Andrew Wang Y, Li L, Wang D, Zhu T, Xu J, Yang C and Li Y 2007 *Nature Photon.* **1** 717
[6] Fang X *et al* 2009 *Adv. Mater.* **21** 2034
[7] Jain F and Huang W 1999 *J. Appl. Phys.* **85** 2706
[8] Dong B, Cao L, Su G, Liu W, Qu H and Jiang D 2009 *J. Colloid Interface Sci.* **339** 78
[9] Kang T, Sung J, Shim W, Moon H, Cho J, Jo Y, Lee W and Kim B 2009 *J. Phys. Chem.* C **113** 5352
[10] José P A, Beatriz J L, Eloisa C, Purificación E, Fabienne P, Bruno V and Clément S 2008 *J. Mater. Chem.* **18** 5193
[11] Hou S, Yuen Y, Mao H, Wang J and Zhu Z 2009 *J. Phys. D: Appl. Phys.* **42** 215105
[12] Wood V, Halpert J E, Panzer M J, Bawendi M G and Bulovic V 2009 *Nano Lett.* **9** 2367
[13] Kar S and Biswas S 2009 *ACS Appl. Mater. Interfaces* **1** 1420
[14] Fang Y, Chu S, Chen H, Kao P, Chen I and Hwang C 2009 *J. Electrochem. Soc.* **156** K55
[15] Surkova T P, Galakhov V R and Kurmaev E Z 2009 *Low Temp. Phys.* **35** 79
[16] Biswas S, Kar S and Chaudhuri S 2005 *J. Phys. Chem.* B **109** 17526
[17] Mandal S K, Mandal A R and Das S 2007 *J. Appl. Phys.* **101** 114315
[18] Ge J, Wang J, Zhang H, Wang X, Peng Q and Li Y 2005 *Adv. Funct. Mater.* **15** 303
[19] Zhuo R F, Feng H T, Yan D, Chen J T, Feng J J, Liu J Z and Yan P X 2008 *J. Cryst. Growth* **310** 3240
[20] Xi G, Wang C, Wang X, Zhang Q and Xiao H 2008 *J. Phys. Chem.* C **112** 1946
[21] Chen X, Xu H, Xu N, Zhao F and Lin W 2003 *Inorg. Chem.* **42** 3100
[22] Liu J, Guo Z, Meng F, Luo T, Li M and Liu J 2009 *Nanotechnology* **20** 125501
[23] Jiang L, Yang M, Zhu S, Pang G and Feng S 2008 *J. Phys. Chem.* C **112** 15281
[24] Li Z, Liu B, Li X, Yu S, Wang L and Hou Y 2007 *J. Phys.: Condens. Matter* **19** 425227
[25] Limaye M V, Gokhale S, Acharya S A and Kulkarni S K 2008 *Nanotechnology* **19** 415602
[26] Kar S, Santra S and Heinrich H 2008 *J. Phys. Chem.* C **112** 4036
[27] Yue G, Yan P, Yan D, Liu J, Qu D, Yang Q and Fan X 2006 *J. Cryst. Growth* **293** 428
[28] Zhao Z, Geng F, Cong H, Bai J and Cheng H 2006 *Nanotechnology* **17** 4731
[29] Cheng C, Xu G, Zhang H, Cao J, Jiao P and Wang X 2006 *Mater. Lett.* **60** 3561
[30] Biswas S, Kar S, Santra S, Jompol Y, Arif M and Khondaker S I 2009 *J. Phys. Chem.* C **113** 3617
[31] Peng X, Manna L, Yang W, Wickham J, Scher E, Kadavanich A and Alivisatos A P 2000 *Nature* **404** 59
[32] Wu Q, Cao H and Zhang S 2006 *Inorg. Chem.* **45** 7316
[33] Wang H, He Y, Ji T and Yan X 2009 *Anal. Chem.* **81** 1615
[34] Koneswaran M and Narayanaswamy R 2009 *Sensors Actuators B: Chem.* **139** 104
[35] Cheng Y, Lu C, Lin Z, Liu Y, Guan C, Lu H and Yang B 2008 *J. Mater. Chem.* **18** 4062
[36] Li Y, Li X, Yang C and Li Y 2004 *J. Phys. Chem.* B **108** 16002
[37] Chai L, Du J, Xiong S, Li H, Zhu Y and Qian Y 2007 *J. Phys. Chem.* C **111** 12658
[38] Albe V, Jouanin C and Bertho D 1998 *Phys. Rev.* B **57** 8778
[39] Hu P, Liu Y, Fu L, Cao L and Zhu D 2004 *J. Phys. Chem.* B **108** 936
[40] Pradhan N and Efrima S 2004 *J. Phys. Chem.* B **108** 11964
[41] Li Z *et al* 2007 *Nanotechnology* **18** 255602
[42] Yao W, Yu S, Pan L, Li J, Wu Q, Zhang L and Jiang J 2005 *Small* **1** 320
[43] Sooklal K, Cullum B S, Angel S M and Murphy C J 1996 *J. Phys. Chem.* **100** 4551
[44] Bhargava R N and Gallagher D 1994 *Phys. Rev. Lett.* **72** 416
[45] Geng B Y, Zhang L D, Wang G Z, Xie T, Zhang Y G and Meng G W 2004 *Appl. Phys. Lett.* **84** 2157
[46] Sapra S, Prakash A, Ghangrekar A, Periasamy N and Sarma D D 2005 *J. Phys. Chem.* B **109** 1663
[47] Tripathi B, Vijay Y K, Wate S, Singh F and Avasthi D K 2007 *Solid State Electron.* **51** 81